remote sensing

MDPI

Article

Existence of Glacier Anomaly in the Interior and Northern Tibetan Plateau between 2000 and 2012

Lin Liu [1], Liming Jiang [2,3,*], Hansheng Wang [2,3] and Yafei Sun [4]

[1] MOE Key Laboratory of Fundamental Physical Quantities Measurement, PGMF and School of Physics, Huazhong University of Science and Technology, Wuhan 430074, China; liulin616@hust.edu.cn
[2] Innovation Academy for Precision Measurement Science and Technology, Chinese Academy of Sciences, Wuhan 430071, China; whs@whigg.ac.cn
[3] University of Chinese Academy of Sciences, Beijing 100049, China
[4] School of Surveying and Urban Spatial Information, Henan University of Urban Construction, Pingdingshan 467036, China; sunyafei@whigg.ac.cn
* Correspondence: jlm@whigg.ac.cn

Abstract: There was sufficient evidence to indicate a nearly balanced glacier mass change (termed glacier anomaly) for Karakoram Mts. since the 1970s, in contrast to worldwide glacier mass losses caused by climate warming. Recently, this anomalous phenomenon was detected over the neighboring western Kunlun and Pamir Mts. However, the southeastern limit of this glacier anomaly remains uncertain, owing to the paucity of glacier mass balance observations across the interior and northern Tibetan Plateau (INTP). In this study, we presented a decadal glacier mass balance estimation in the INTP by differencing the SRTM DEM with the topographic data produced from TanDEM-X bistatic InSAR images. From 2000 to 2012, decade-average glacier mass balances of between -0.339 ± 0.040 and 0.237 ± 0.078 m w.e. yr^{-1} were detected over 22 glacierized areas. Significantly, we found a gradient and switch of glacier mass loss over the southeastern portion to glacier mass gain over the northwestern portion. This varying spatial pattern illustrates that glacier anomaly has existed over the northwestern or even central zone of the INTP since the early 21st century. This study provides important evidence for the model simulation of both glacier evolution and atmospheric circulations in investigating the prevailing mechanism of the regional anomalous phenomenon.

Keywords: glacier anomaly; glacier mass balance; TanDEM-X bistatic InSAR; interior and northern Tibetan Plateau; High Mountain Asia

Citation: Liu, L.; Jiang, L.; Wang, H.; Sun, Y. Existence of Glacier Anomaly in the Interior and Northern Tibetan Plateau between 2000 and 2012. *Remote Sens.* **2022**, *14*, 2962. https://doi.org/10.3390/rs14132962

Academic Editors: Sergey V. Popov, Gang Qiao, Xiangbin Cui and Nikola Besic

Received: 28 April 2022
Accepted: 19 June 2022
Published: 21 June 2022

1. Introduction

Glacier meltwater induced from the mass loss of glacierized regions over the High Mountain Asia (HMA) is a significant contributor to global sea level rise [1,2]. On a regional scale, the decadal expansion of lakes over the Tibetan Plateau (TP) is partly caused by glacier melting [3,4]. Furthermore, glacier melting provides an important freshwater supply for billions of people living in the eastern, southern and central parts of Asia [5,6]. Especially in drought years, more than 50% of the annual runoff in most catchments of the HMA is supplied by glacier mass loss [6].

With the warming climate, most glacierized regions in the HMA experienced continuous glacier mass losses in the past several decades [7]. However, an anomalous phenomenon refers that a balanced/positive mass change was first noted in the glaciers of the Karakoram Mts. [8]. Moreover, the glacier anomaly has been found to exist over the Pamir [9] and western Kunlun Mts. [10]. For the large-scale glacier anomalous areas, the Pamir–Karakoram–western Kunlun (PKWK) glacier anomaly is proposed to be possibly induced by regional precipitation increase [11]. Furthermore, previous studies generally

agreed that the western region of the Pamir–Karakoram Mountains is the possible northwestern boundary of the PKWK glacier anomaly [10,11]. However, the center of the glacier anomaly remains controversial, with candidates such as the eastern Pamir [12], the western Kunlun Mts. [11] and the southwestern margins of the Tarim Basin [10]. This debate is still ongoing due to limited understanding of the existence of glacier anomaly in the interior and northern Tibetan Plateau (INTP).

For a small amount of water-vapor transported from atmospheric circulations, glaciers are sparse in the mountainous areas of the INTP [13]. Therefore, techniques of satellite gravimetry (e.g., GRACE) and laser altimetry (e.g., ICESat) are seriously limited in the INTP. Specifically, the GRACE observation is insensitive to the sparse mountain glaciers and it is challenging to separate the glacier mass budget from the measured terrestrial water storage variations [14]. Moreover, for employing the ICESat observations to detect mass changes in small glaciers in the mid-latitude areas, the considerable bias and uncertainty can be caused by insufficient spatial sampling [15]. Accordingly, very few glacierized regions (e.g., the western Kunlun and Nainqentanglha Mts.) have been measured by ICESat data over the INTP [16].

To the best of our knowledge, few field measurements of glacier mass change have been made in the INTP during recent decades. Only three glaciers, namely Xiaodongkemadi, Zhadang and Gurenhekou, have been field measured for more than three consecutive years [17]. By using the elevation change trend calculated from multi-temporal ASTER DEMs, the regional-wide glacier mass change of -0.19 ± 0.08 m w.e. yr^{-1} (2000–2016) was detected in the inner Tibet [18]. Recently, Shean et al. (2020) employed similar data and method to retrieve glacier mass change in the Tibetan interior mountains at -0.12 ± 0.05 m w.e. yr^{-1} in 2000–2018 [7]. However, mapping surface topography in the glacial zone is still a challenge for optical photogrammetry due to the lack of radiometric contrast on snow and firn. The limited quota of snow-free and cloud-free optical images can lead to an additional systematic bias for glacier mass balance estimates in INTP.

The geodetic method comparing two DEMs at different time epochs has been used extensively to detect decade-average glacier mass balances in the HMA [19,20]. For the INTP, however, detailed measurements of glacier mass balance on a large scale are still scarce. A few glacierized areas such as the Puruogangri ice field and Geladandong Mts. have been investigated for estimating glacier mass changes in recent decades. By comparing the TanDEM-X DEM with the SRTM DEM, a slightly negative glacier mass change of -0.038 ± 0.023 m w.e. yr^{-1} was observed between 2000 and 2012 in the Puruogangri ice field [21]. With the similar data processing strategy, glacier mass changes of -0.235 ± 0.127, -0.12 ± 0.22 and 0.128 ± 0.055 m w.e. yr^{-1} were estimated for the period 2000–2014 in the Geladandong Mts. [22], western Nainqentanglha Mts. [23] and western Kunlun Mts. [10], respectively.

This study seeks to carefully investigate the spatial variations in glacier mass changes in recent decades in the INTP. The SRTM DEM was compared with DEMs derived from TanDEM-X InSAR data to accurately determine glacier elevation changes over 22 glacierized areas. In order to estimate the decade-average glacier mass balance, the systematic biases of the C/X-band radar penetration difference and seasonal glacier mass changes were corrected for each study site. Importantly, the spatial pattern of glacier mass balances for these study sites was analyzed to identify the glacier anomalous regions in the INTP. Furthermore, combining our results with the previously published geodetic glacier mass balance estimates, we discussed the possible center of the glacier anomaly in the HMA and the influence of atmospheric circulations in the TP.

2. Study Area

The INTP, consisting mainly of the endorheic basin of the TP, is located in the east of the Karakoram Mts. and in the north of the Tarim Basin. The extent of the INTP is about 80°E–93°E and 29°N–37°N (Figure 1). The average elevation of the INTP is more than 4400 m a.s.l. with mountain peaks such as Songzhi peak and Muztagh peak exceeding

6000 m a.s.l. The central area of the INTP (30°N–35°N) is referred to as the transitional region between the Indian summer monsoon and mid-latitude westerlies [24]. However, the adjacent high mountains trap water-vapor transport from these two atmospheric circulations [25]. Basically, continental climate processes dominate the climate of the INTP, which is characterized by dryness and cold [17]. The annual precipitation of the INTP is about 200–500 mm and the yearly average air temperature over the glacier equilibrium-line altitude is ~−10.0 °C [26].

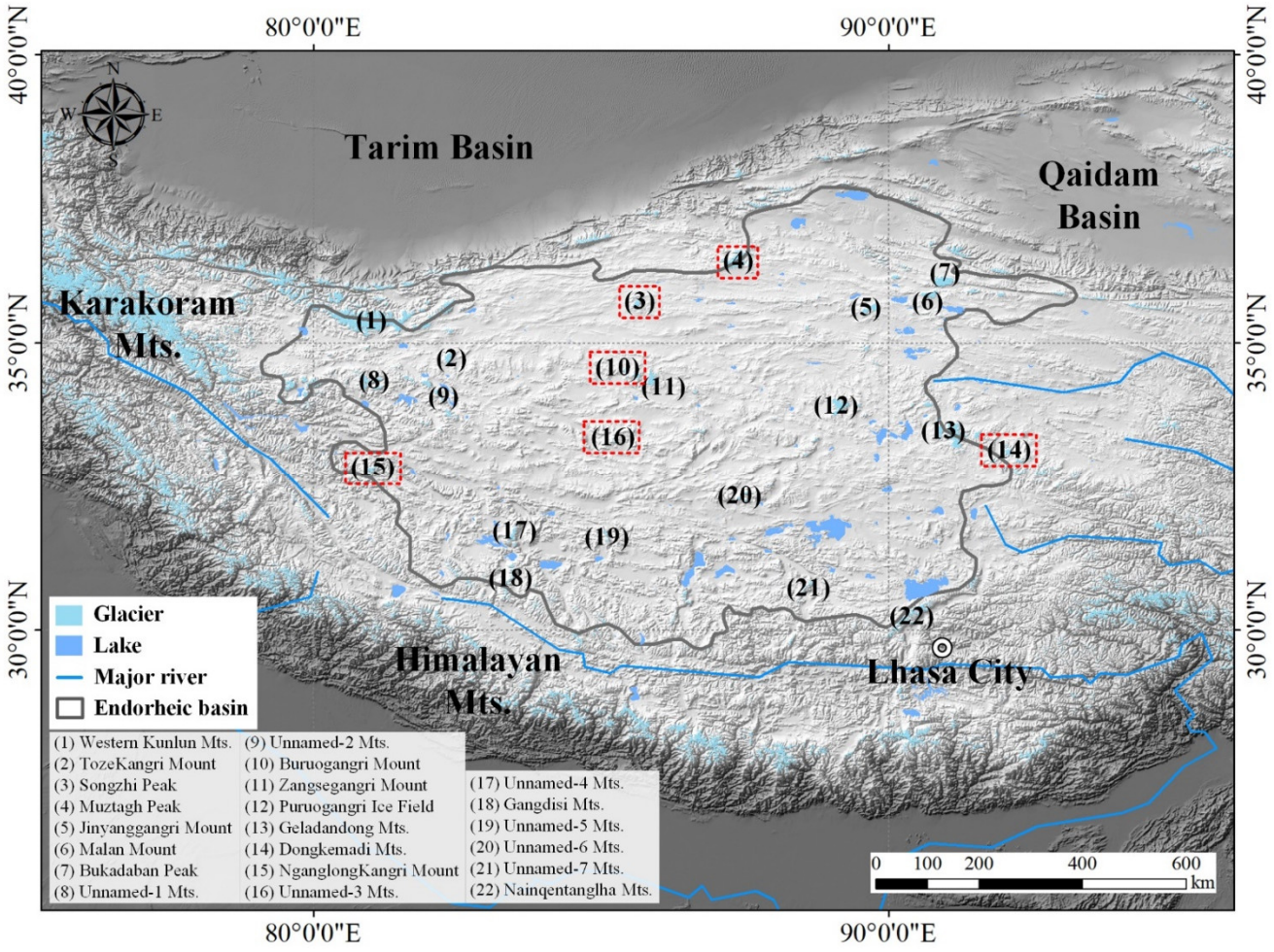

Figure 1. Geographic locations of the 22 study areas over the INTP. The six study sites completely covered by the SRTM-X DEM are labeled by red dashed rectangles. The mountain glaciers are shown in light blue. Gray solid line indicates the boundary of the endorheic basin.

Mountain glaciers are characterized by sparse distribution and small size in the INTP. The second Chinese Glacier Inventory (SCGI) indicates that the area of more than 75% of the glaciers in the INTP is smaller than 1.0 km^2 [13]. As shown in Figure 1, modern glaciers only exist on a few mountains in this region. In this study, 22 glacierized core areas were selected for representing the spatial variations in glacier mass balances in the INTP (Figure 1). Most of the meltwater from the glaciers in these 22 glacierized areas flows into the endorheic basin, supplying water to Asia's major rivers such as the Yellow River and the Yarlung Zangbo River. In recent decades, the water level and volume of many endorheic lakes has increased [27,28], partly resulting from glacier meltwater [29,30]. From the 1970s to 2009, glaciers in the INTP generally experienced a steady terminus retreat [31]. Moreover, between 2000 and the 2010s, a negative glacier mass change was observed in some glacierized regions such as the Puruogangri ice field [21], western Nyainqentanglha Mts. [23] and central Kunlun Mts. [32].

3. Data and Methods

3.1. Single-Pass InSAR DEMs

We employed two single-pass space-borne InSAR DEMs to estimate glacier elevation changes in these 22 glacierized areas over the INTP (Table 1). The more recent DEMs were extracted from 34 pairs of TanDEM-X bistatic InSAR data between February 2011 and March 2014. The format of raw TanDEM-X single look complex (SLC) data collected from the German Aerospace Center is CoSSC, which indicates that each pair of bistatic InSAR data has been co-registered. The spatial resolution of TanDEM-X data is ~2 m in the azimuth and range directions. Here, we employed the SAR interferometric processing strategy to generate 30 m spatial resolution DEMs for each study site from the raw TanDEM-X SLC images [33].

Table 1. The used SRTM DEM and TanDEM-X bistatic InSAR data in this study.

Name of Study Site	No. of Study Site in Figure 1	DEM in 2000	TanDEM InSAR Data (Pair)
Western Kunlun Mts.	1	SRTM-C DEM	1
Tozekangri Mount	2	SRTM-C DEM	1
Songzhi Peak	3	SRTM-X DEM	1
Muztagh Peak	4	SRTM-X DEM	1
Jinyanggangri Mount	5	SRTM-C DEM	1
Malan Mount	6	SRTM-C DEM	2
Bukadaban Peak	7	SRTM-C DEM	1
Unnamed-1 Mts.	8	SRTM-C DEM	1
Unnamed-2 Mts.	9	SRTM-C DEM	1
Buruogangri Mount	10	SRTM-X DEM	6
Zangsegangri Mount	11	SRTM-C DEM	1
Puruogangri Ice Field	12	SRTM-C DEM	2
Geladandong Mts.	13	SRTM-C DEM	1
Dongkemadi Mts.	14	SRTM-X DEM	1
NganglongKangri Mount	15	SRTM-X DEM	2
Unnamed-3 Mts.	16	SRTM-X DEM	3
Unnamed-4 Mts.	17	SRTM-C DEM	1
Gangdisi Mts.	18	SRTM-C DEM	3
Unnamed-5 Mts.	19	SRTM-C DEM	1
Unnamed-6 Mts.	20	SRTM-C DEM	1
Unnamed-7 Mts.	21	SRTM-C DEM	1
Nainqentanglha Mts.	22	SRTM-C DEM	1

The earlier glacier surface topographies were derived from the 30 m resolution SRTM DEM taken during an 11-day mission in February 2000. In recent years, two SRTM DEMs have been released. The SRTM-X DEM was created using the X-band SAR images and the C-band SAR interferometric data were used to produce the SRTM-C DEM. While the SRTM-X DEM has better vertical and horizontal accuracy than the SRTM-C DEM, it cannot provide complete spatial coverage for all 22 sites due to the discrete passing swaths (i.e., 50 km) [34]. Therefore, we preferred to utilize the SRTM-X DEM with complete coverage of the six study sites (Figure 1) and the remaining 16 glaciers were compared with SRTM-C DEM products.

3.2. Glacier Elevation Change Calculation

The SRTM-C/X DEM (2000) was compared with the generated TanDEM-X DEMs (2011–2014) to retrieve the elevation changes in the 22 study areas. Prior to the DEM differential operation, the universal co-registration technique was performed for eliminating the vertical discrepancy from the horizontal deviations [35], ensuring that all pairs of TanDEM-X DEM and SRTM DEM could be accurately matched. In addition, the systematic errors between a pair of DEMs related to terrain parameters such as altitude, slope and curvature were corrected with polynomial functions. For example, in order to remove

the systematic error related to slope, we used a polynomial fit of elevation difference as a function of slope. Glacier surface elevation changes in each study site were detected by DEM differencing with the glacier boundaries from the SCGI. Basically, the SCGI glacier outlines were delineated from Landsat optical scenes acquired around 2006–2010 [13]. Here, taking into consideration the continuous glacier terminus retreat in recent decades [31], we used the cloud-free Landsat data in 1999 or 2000 to manually modify the terminus positions of non-surge glaciers. Moreover, the terminus locations of surge-type glaciers, especially for those experiencing a surging event within our study period, were manually updated with Landsat optical images referring to the acquisition date of our used bistatic SAR interferometric data.

The measured glacier surface elevation changes cannot be directly converted into glacier mass balance due to data void and outliers. Specifically, some data gaps were existed for the original SRTM-C/X DEM over the mountainous regions. Therefore, it is necessary to calculate the mean value of glacier elevation changes for each glacierized region. In order to accurately compute glacier-wide average elevation change, we excluded the interpolated pixels located on the void areas of the original SRTM-C/X DEM and removed the pixels on steep surfaces with a slope angle larger than 25 degrees [33]. Moreover, we did not employ the elevation differences of greater than $\pm$100 m over non-surge glaciers. In addition, the threshold of elevation changes was set to $\pm$150 m for surge-type glaciers. For determining these two above thresholds, we analyzed our observed maps of DEM differencing and investigated the previously published results of glacier elevation changes over the INTP [16,32].

Considering that the glacial surface pixels at a specific altitude range are supposed to maintain spatially continuous feature [36], we statistically calculated the average glacier elevation change in each study site with 50 m altitude interval. By using the pixels with different elevation changes within three standard deviations of the average value, the influence of random errors was minimized and thus the average elevation change in an altitude band was calculated accurately. Since the elevation changes with altitude between non-surge and surge-type glaciers have different characteristics [8], surge-type glaciers could be excluded from the estimation. Here, we calculated the average elevation change in each surge-type glacier separately. Overall, for a study site with partly surge-type glaciers, the average glacier elevation change was calculated as an area-weighted mean value over all surge-type and non-surge glaciers.

3.3. Glacier Mass Balances Estimation

3.3.1. C/X-Band Radar Signal Penetration Difference

By using the density of 850 kg m^{-3} [37], we converted the calculated average value of glacier elevation changes into glacier mass balance. However, the results observed directly from the TanDEM-X DEMs and SRTM-C DEM may be biased because of the different capacities of C/X-band radar signal when penetrating into glacier surface. In general, C-band radar wave has the penetration depth of about several meters over the glacierized areas of the HMA [38], whereas that of X-band radar wave is typically not more than 1 m [39,40]. Therefore, according to site-by-site penetrating characteristics, we carefully estimated the penetrating depth difference term with a comparison between the SRTM-X and SRTM-C DEMs over each study site.

Considering the variations in penetration depth differences over various glacier surfaces (e.g., ice, firn and snow), the average penetration difference of a study site was accurately calculated for 50 m altitude bands. Similar to the calculation of the average glacier elevation change, we only used pixels where the penetration differences did not deviate more than three standard deviations from the average value over each altitude band. It is noteworthy that the available data of SRTM-X DEM are significantly limited in the INTP due to the discrete swaths with the width of 50 km [34]. Therefore, for a study site without X-band SRTM DEM (e.g., the Tozekangri Mountain, Geladandong Mts. and Bukadaban Mountain), we referred the penetration difference to the nearest study site.

3.3.2. Seasonality Correction

In this study, the raw InSAR images of the SRTM DEM were derived in mid-February, whereas the used TanDEM-X bistatic InSAR images were acquired between mid-October and late June (Table 1). Thus, the seasonal glacier mass change in one to four months in winter or spring (depending on the study site) is a possible systematic bias for estimating the decade-average glacier mass balance. According to the seasonality of precipitation, the glaciers of our 22 study sites are classified into three accumulation regimes of winter/spring accumulation, spring/summer accumulation and summer accumulation [26]. For winter/spring accumulation glaciers in the INTP, we employed the seasonal corrections which were estimated by using the TanDEM-X InSAR images collected in different months in the western Kunlun Mts. [10]. Specifically, the corrections of 0.24, 0.18, 0.12, 0.06, −0.06, −0.12 and −0.18 m w.e. were applied in October, November, December, January, March, April and May, respectively. Moreover, we used the correction of zero in the winter months and −0.06, −0.12 and −0.18 m w.e. in March, April and May over the glaciers of spring/summer accumulation. In addition, since both glacier melting and snowfall majorly occur in summer season [41], no seasonal glacier mass change was modified for all summer accumulation glaciers in the INTP. Notably, the used TanDEM-X InSAR data of the NganglongKangri Mount (winter/spring accumulation type) were acquired on 26 June. Here, we assumed that the glacier mass gain between March and May is possibly compensated by the negative glacier mass change in June. Thus, the correction of seasonal variations was set to zero for the NganglongKangri Mount.

3.3.3. Decade-Average Glacier Mass Balance Estimation

Overall, for a study site, the estimation of decade-average glacier mass balance (ΔB) was summarized as the following Equation (1). It is noteworthy that more than half of the used TanDEM-X bistatic InSAR images were collected between November 2011 and May 2012. Therefore, in this study, the inter-annual variation was neglected and the estimated results were reasonably assumed to represent the decade-average glacier mass balances in 2000–2012.

$$\Delta B = \frac{(dh\text{-}P_{diff}) \times \rho_{glac}/\rho_w + \Delta B_{season}}{T}, \quad (1)$$

where T denotes the integral number of years of our studied periods; ρ_w denotes the water density (1000 kg m^{-3}); P_{diff} is the calculated mean value of radar signal penetration difference; ρ_{glac} (850 kg m^{-3}) is our used glacial density; dh represents our observed average glacier elevation change; and ΔB_{season} is the seasonal correction of glacier mass change.

3.4. Uncertainty Analysis

According to Equation (1), the uncertainty of glacier mass balance is related to the errors of the average glacier elevation change, radar penetration difference, glacial density and seasonal glacier mass change.

$$\sigma_{\Delta B} = \frac{\sqrt{(dh\text{-}P_{diff})^2 \times \sigma^2_{\rho_{glac}}/\rho^2_w + \left(\sigma^2_{dh} + \sigma^2_{P_{diff}}\right) \times \rho^2_{glac}/\rho^2_w + \sigma^2_{\Delta B_{season}}}}{T}, \quad (2)$$

where $\sigma_{\rho_{glac}}$ denotes the error of glacial density and is about 7% of our used glacial density [37]. $\sigma_{\Delta B_{season}}$ denotes the error of seasonal corrections. Here, we conservatively assumed a 100% error for the correction of seasonal mass change. Furthermore, the error of seasonal variation in summer accumulation glaciers was assumed to be the mean value of the calculated uncertainties over the study sites with seasonal corrections. $\sigma_{P_{diff}}$ represents the error of our calculated radar penetration difference and σ_{dh} denotes the error of our detected average glacier elevation change. Here, these two errors were estimated by the standard law of error propagation [42]. In addition, for the study site (e.g., the Tozekan-

gri Mount and Bukadaban peak) with no SRTM-X DEM, we assumed that the error of C/X-band radar penetration difference is twice that of the nearest study site.

4. Results

4.1. Glacier Elevation Changes

The results obtained from the comparison between TanDEM-X DEMs and SRTM-X/C DEM are exhibited in Figures 2–6 for the 22 study sites in the INTP. In this study, a non-negligible systematic error of radar penetration difference is present in the results estimated with TanDEM-X DEM and SRTM-C DEM. Therefore, the spatial pattern of our observed glacier elevation changes was demonstrated using the six study sites with complete coverage by SRTM-X DEM (Figure 2). Over these six glacierized regions, we detected a pronounced surface lowering at most of the glacier ablation zones (locally exceeding −60 m), whereas an increase in ice thickness (not more than 30 m) was observed over the high accumulation zones. In contrast, the surface of the central Yulinchuan Glacier was significantly thickened at the terminus and an apparent surface thinning was found over the upper areas (Figure 2e). This extraordinary pattern of glacier elevation changes between 2000 and the 2010s is probably attributed to a surging event over this glacier from 2008 to 2009 [43].

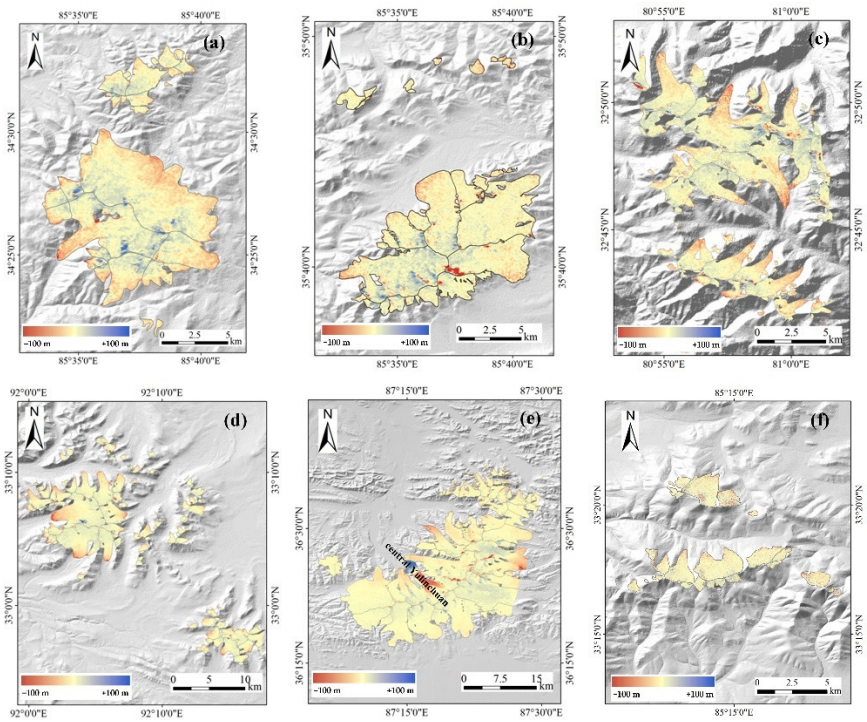

Figure 2. The maps of the observed glacier elevation changes from 2000 to the 2010s over the six study sites with a complete coverage of the SRTM-X DEM (See Figure 1, red rectangle areas). (**a**) Buruogangri Mount; (**b**) Songzhi peak; (**c**) NganglongKangri Mount; (**d**) Dongkemadi Mts.; (**e**) Muztagh peak; (**f**) Unnamed-3 Mts. The central Yulinchuan Glacier experienced a surging event from 2008 to 2009.

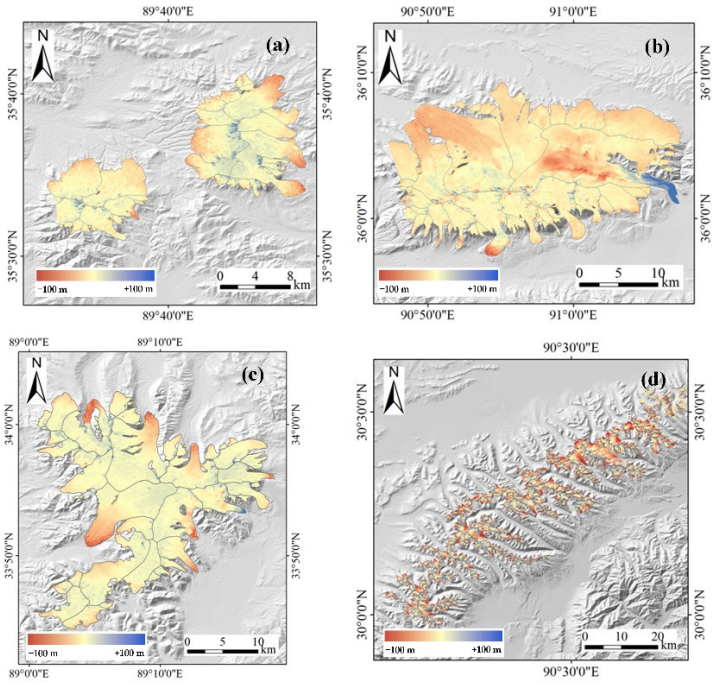

Figure 3. The observed maps derived by subtracting the SRTM-C DEM from the TanDEM-X DEMs over the study sites of Jinyanggangri Mount (**a**), Bukadaban peak (**b**), Puruogangri ice field (**c**) and Nainqentanglha Mts. (**d**).

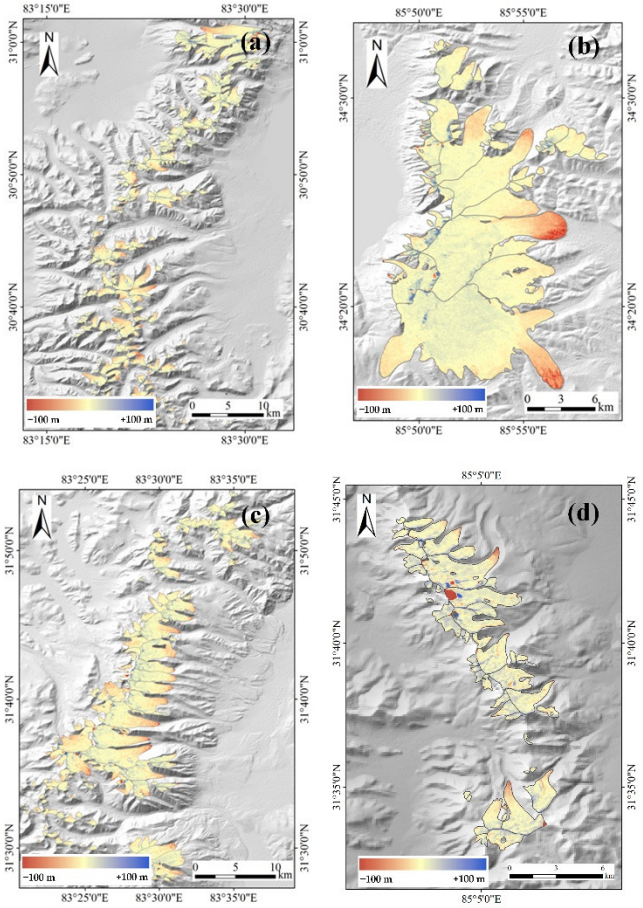

Figure 4. Same as Figure 3 but for the study sites of Gangdisi Mts. (**a**), Zangsigangri Mount (**b**), Unnamed-4 Mts. (**c**) and Unnamed-5 Mts. (**d**).

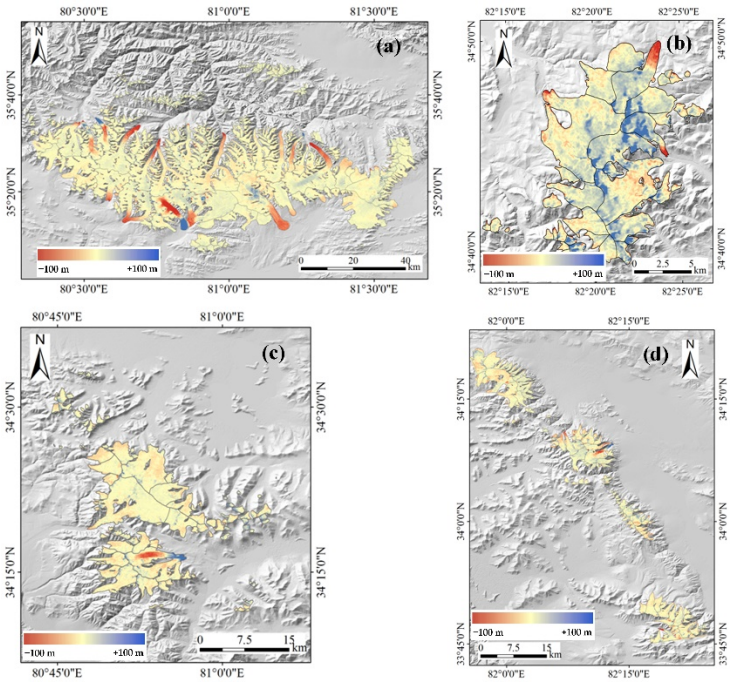

Figure 5. Same as Figure 3 but for the study sites of western Kunlun Mts. (**a**), Tozekangri Mount (**b**), Unnamed-1 Mts. (**c**) and Unnamed-2 Mts. (**d**).

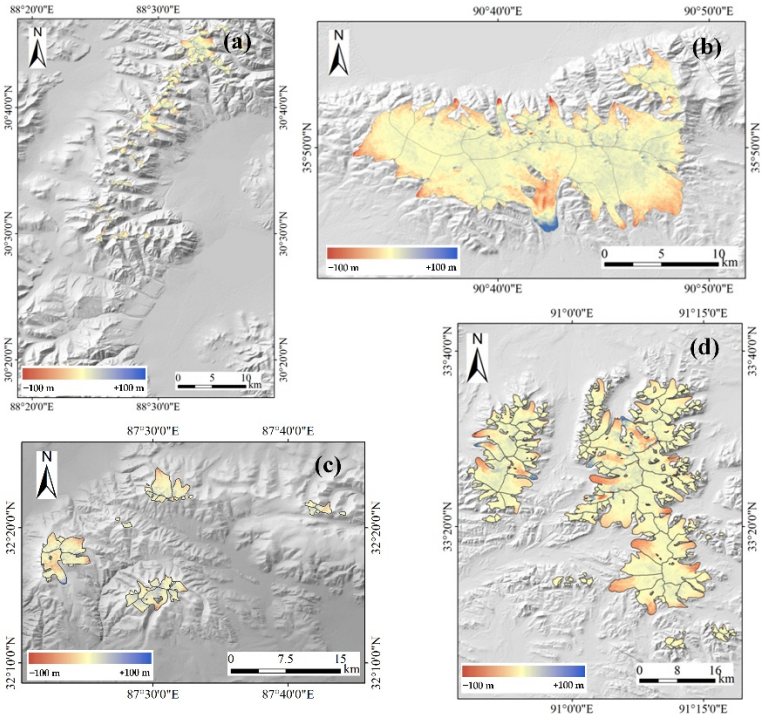

Figure 6. Same as Figure 3 but for the study sites of Unnamed-7 Mts. (**a**), Malan Mount (**b**), Unnamed-6 Mts. (**c**) and Geladandong Mts. (**d**).

For non-surge glaciers on these six glacierized areas, the glacier elevation changes are proportional to altitudes (Figure 7). In general, over the lower zones, we measured a decreasing trend of glacier surface thinning with altitude. Moreover, a probably increasing tendency of glacier surface thickening with altitude was observed at the upper zones. The observed altitude-dependent glacier elevation relationship is also consistent with the meteorology conditions in the INTP (e.g., precipitation and temperature) [44]. In addition,

we found that both glacier surface thinning and thickening rates of the Dongkemadi Mts. are relatively larger than the other five study sites (Figure 7), which may be attributed to the only case of summer-accumulation type among the six sites.

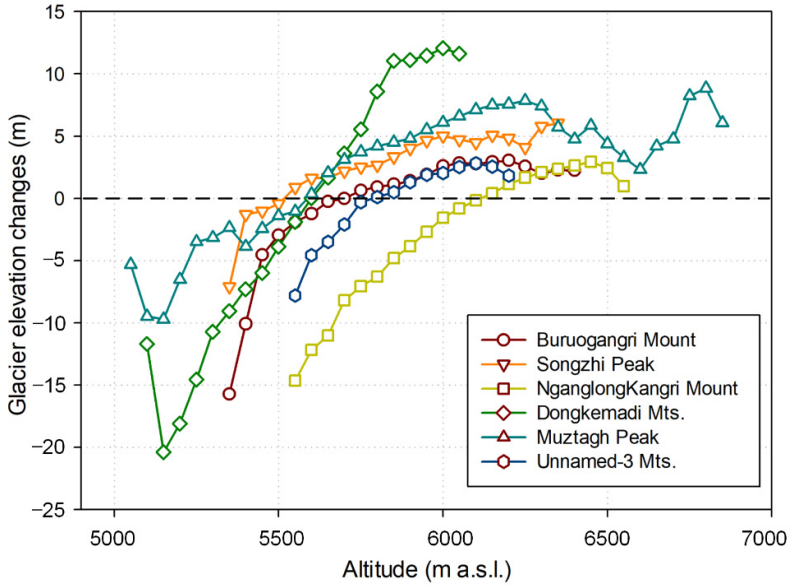

Figure 7. Glacier elevation changes versus altitude for the six study sites completely covered by X-band SRTM DEM (See Figure 1, red rectangle areas).

4.2. Spatial Variation in Glacier Mass Balances

Between 2000 and 2012, glacier mass balances were found to be heterogeneous in the INTP. Over the 22 study sites, we estimated decade-average mass changes of between -0.339 ± 0.040 and 0.237 ± 0.078 m w.e. yr^{-1} (Table 2). In general, nine study sites (e.g., the Songzhi peak and western Kunlun Mts.) experienced positive glacier mass balances, whereas mass losses can be detected for the other thirteen glacierized areas such as the Nainqentanglha and Geladandong Mts. The most serious negative mass change observed was -0.339 ± 0.040 m w.e. yr^{-1} on the Dongkemadi Mts. situated in the southeastern portion of the INTP. The Tozekangri Mount located in the northwestern region of the INTP experienced the largest glacier mass gain. Overall, for all these 22 glacierized regions in the INTP, we derived a mean mass change of 0.018 ± 0.021 m w.e. yr^{-1} between 2000 and 2012.

As exhibited in Figure 8, the spatial variation in our measured glacier mass balances was clearly characterized by glacier mass gain for the northwestern part and glacier mass loss for the southeastern part. Therefore, with a visual interpretation of the glacier mass balance estimates, we divided the INTP into the three sub-areas of zone A (northwestern part), zone B (central part) and zone C (southeastern part). In zone A, we estimated positive glacier mass changes of between 0.058 ± 0.037 and 0.237 ± 0.078 m w.e. yr^{-1} for the six study sites (Table 2). Moreover, for all the eight glacierized regions in zone C, we detected the negative glacier mass changes. However, as illustrated in Table 2, the observed mass balances of zone B varied. Over this central zone, glaciers in the study sites of the Buruogangri Mount, Jinyanggangri Mount and Unnamed-3 Mts. basically experienced mass gains, whereas glacier mass loss was estimated on the other five glacierized areas such as Bukadanban peak, Malan Mount and NganglongKangri Mount (Figure 8).

Table 2. The estimated glacier mass changes on the 22 glacierized areas of the INTP between 2000 and 2012. The "N/A" indicates that the corrections of seasonal variations or C/X-band radar penetration differences are not needed for a study site. The number. of each study site is shown in Figure 8.

No.	Study Site	Mean Elevation Change (m)	Penetration Correction (m)	Seasonal Correction (m w.e.)	Mass Balance (m w.e. yr^{-1})
A1	Western Kunlun Mts.	4.11 ± 0.37	2.67 ± 0.46	0.15 ± 0.15	0.116 ± 0.050
A2	Unnamed-1 Mts.	2.83 ± 0.20	1.83 ± 0.53	−0.04 ± 0.04	0.058 ± 0.037
A3	Tozekangri Mount	4.96 ± 0.37	2.35 ± 1.12	0.00 ± 0.10	0.237 ± 0.078
A4	Unnamed-2 Mts.	4.50 ± 0.28	2.35 ± 0.56	−0.12 ± 0.12	0.131 ± 0.048
A5	Songzhi Peak	2.70 ± 0.56	N/A	N/A	0.191 ± 0.042
A6	Muztagh Peak	1.03 ± 0.27	N/A	0.00 ± 0.10	0.063 ± 0.019
B1	NganglongKangri Mount	−1.49 ± 0.30	N/A	0.00 ± 0.10	−0.106 ± 0.024
B2	Unnamed-4 Mts.	1.13 ± 0.18	1.39 ± 0.51	N/A	−0.016 ± 0.032
B3	Unnamed-3 Mts.	0.46 ± 0.15	N/A	−0.03 ± 0.03	0.033 ± 0.012
B4	Buruogangri Mount	0.78 ± 0.22	N/A	N/A	0.055 ± 0.016
B5	Zangsegangri Mount	2.27 ± 0.21	2.79 ± 0.46	−0.03 ± 0.03	−0.036 ± 0.037
B6	Jinyanggangri Mount	3.13 ± 0.28	2.05 ± 0.68	0.00 ± 0.10	0.077 ± 0.056
B7	Malan Mount	−0.65 ± 0.10	2.05 ± 1.36	−0.03 ± 0.03	−0.194 ± 0.097
B8	Bukadaban Peak	0.76 ± 0.13	2.05 ± 1.36	−0.30 ± 0.30	−0.116 ± 0.101
C1	Gangdisi Mts.	−0.60 ± 0.16	1.39 ± 1.02	N/A	−0.121 ± 0.063
C2	Unnamed-5 Mts.	0.72 ± 0.18	1.39 ± 1.02	N/A	−0.041 ± 0.063
C3	Unnamed-6 Mts.	1.70 ± 0.26	2.23 ± 0.66	N/A	−0.032 ± 0.045
C4	Unnamed-7 Mts.	0.12 ± 0.27	1.58 ± 0.82	N/A	−0.089 ± 0.053
C5	Nainqentanglha Mts.	−0.44 ± 0.32	1.58 ± 0.41	0.00 ± 0.10	−0.135 ± 0.033
C6	Puruogangri Ice Field	1.95 ± 0.20	2.23 ± 0.33	N/A	−0.020 ± 0.031
C7	Geladandong Mts.	0.43 ± 0.13	2.23 ± 0.66	0.00 ± 0.10	−0.128 ± 0.050
C8	Dongkemadi Mts.	−4.79 ± 0.46	N/A	N/A	−0.339 ± 0.040

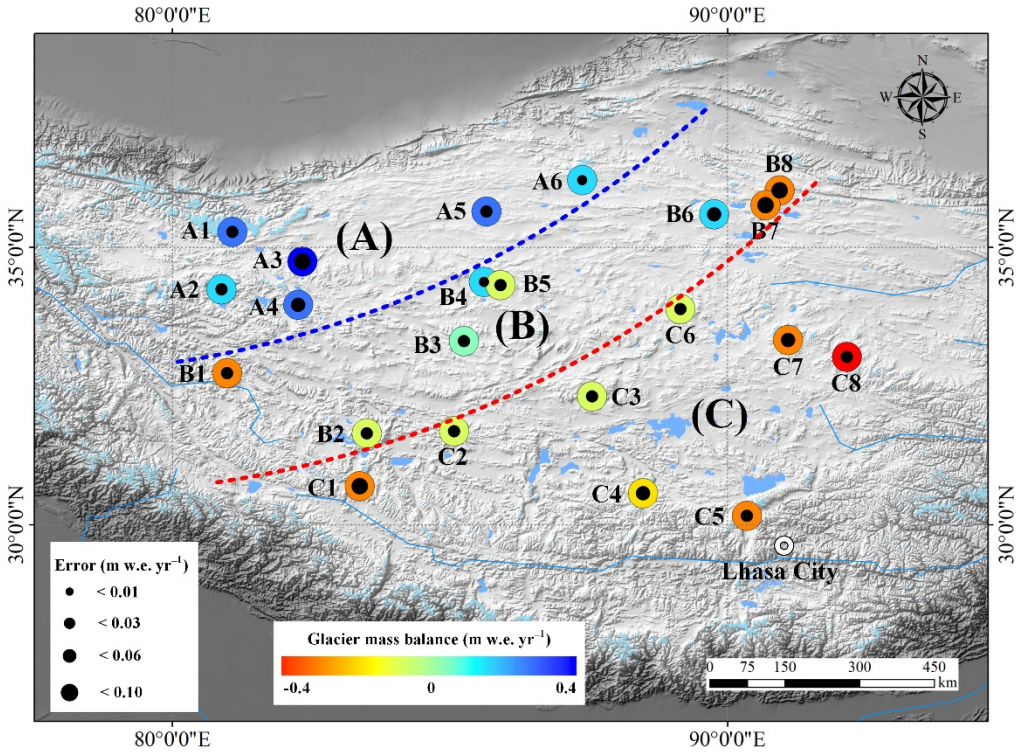

Figure 8. The estimated decade-average (2000–2012) glacier mass balance of the 22 study areas over the INTP. The blue and red dashed lines are used to divide the INTP into three sub-regions of zone A, B and C.

The detected spatial feature of glacier mass change is also basically supported by the correlation between latitude/longitude and mass balance of the 22 study sites (Figure 9). Specifically, a pronounced positive correlation was retrieved for glacier mass balance and latitude (Figure 9a). Moreover, all the study sites located on the south of 33°N experienced glacier mass losses from 2000 to 2012. For the relationship between glacier mass balance and longitude, our results demonstrated a negative correlation. It indicates that these study sites located over the eastern portion of the INTP possibly experienced less glacier mass gain (or more glacier mass loss) than the western counterpart. The maximum of glacier mass loss was detected on the easternmost study site (Figure 9b).

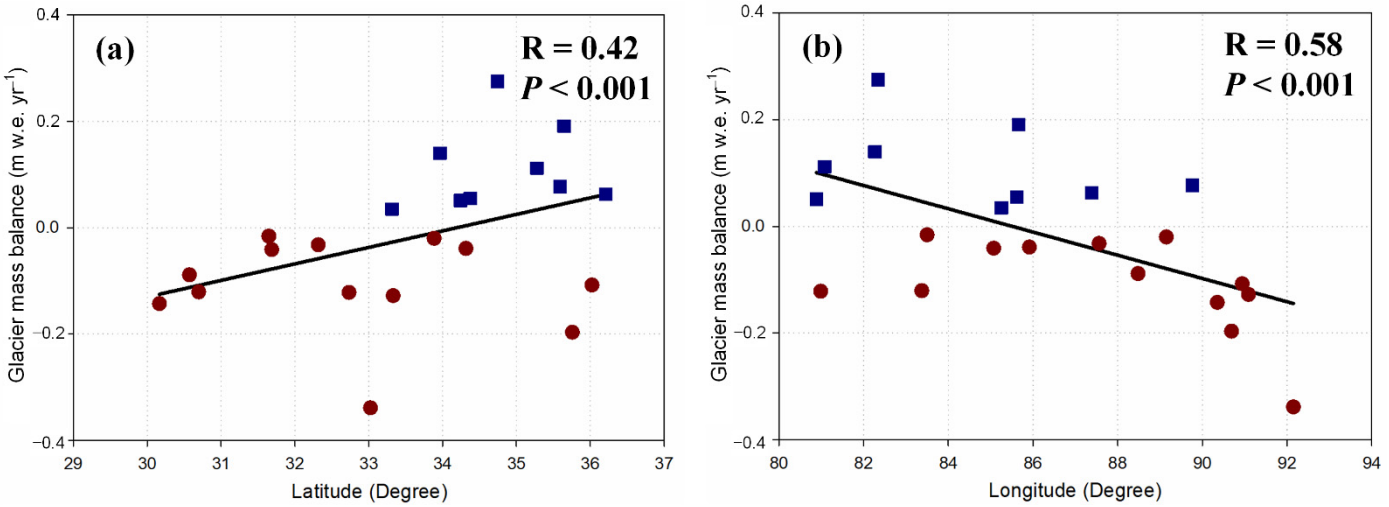

Figure 9. The correlation between glacier mass change and latitude (**a**) and longitude (**b**) for these 22 study sites in the INTP. The study site experienced a glacier mass gain from 2000 to 2012, which is indicated as a blue rectangle. The dark red circles represent the study sites with a negative glacier mass change during the studied period.

5. Discussion

5.1. Comparison to Previously Published Estimates

We compared our measured glacier mass changes to previously published results for individual glaciers, study sites and the entire INTP. Throughout the INTP, the glacier mass balances of the individual glaciers of Zhadang, Gurenhekou and Xiaodongkemadi were measured with in situ observations between 2000 and 2012. By employing the standard deviation as the uncertainty of mean glacier mass change, field measured glacier mass balances were -0.591 ± 0.709 (2005–2008), -0.312 ± 0.524 (2005–2010) and -0.358 ± 0.370 (2000–2010) m w.e. yr^{-1} on the glaciers of Zhadang, Gurenhekou and Xiaodongkemadi, respectively [17]. To compare with field measurements, the mass changes in these three glaciers were estimated separately. In general, our estimated glacier mass balances agree with in situ observations (Figure 10). For example, on the Xiaodongkemadi Glacier, our geodetic estimate is -0.310 ± 0.056 m w.e. yr^{-1}, a value that, although indicates less mass loss, is nevertheless in agreement with field measurements (-0.358 ± 0.370 m w.e. yr^{-1}).

At the spatial scale of study sites, Figure 10 indicates that our observed glacier mass balances also agree well with the previously published geodetic estimates in the Nainqentanglha Mts. [23], Geladandong Mts. [22], western Kunlun Mts. [10], Puruogangri ice field [21], Malan Mount and Bukadaban peak [32]. Furthermore, based on the repeat footprints of ICESat altimetry and SRTM-C DEM, the glacier mass changes of 0.14 ± 0.14, 0.03 ± 0.25 and 0.04 ± 0.06 m w.e. yr^{-1} between 2003 and 2008/2009 were estimated over the western Kunlun Mts. [11,14,16]. Basically, these results are consistent with our glacier mass balance estimation in this glacierized region. In the study site of Nyainqentanglha Mts., our measured glacier mass balance is also basically supported by the result derived

from satellite laser observations (-0.20 ± 0.29 m w.e. yr^{-1}) [16]. However, for the study sites of Zangsegangri Mount and Songzhi peak, our estimated glacier mass change is much smaller than that observed by ICESat (0.37 ± 0.25 m w.e. yr^{-1}). This significant difference is probably attributed to the insufficient spatial coverage of ICESat ground tracks in mid-latitude regions.

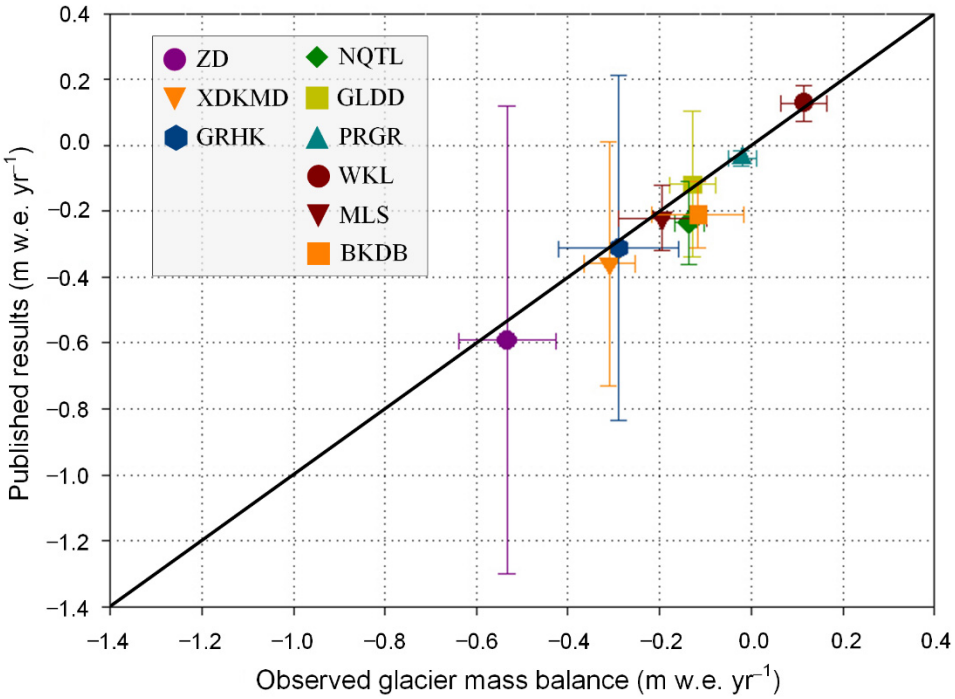

Figure 10. The comparison between our glacier mass change estimations and the field measured results over the individual glaciers of ZD, XDKMD and GRHK, and the published geodetic results over the six study sites of NQTL, GLDD, PRGR, WKL, MLS and BKDB. (ZD: Zhadang Glacier; XDKMD: Xiao Dongkemadi Glacier; GRHK: Gurenhekou Glacier; NQTL: Nainqentanglha Mts.; GLDD: Geladandong Mts.; PRGR: Puruogangri Ice Field; WKL: Western Kunlun Mts.; MLS: Malan Mount; BKDB: Bukadaban peak).

For the entire INTP, the comparison between our glacier mass balance estimations and previously published results is complicated because of differences in the time period and spatial coverage. In this study, we calculated a decade-average glacier mass balance of 0.018 ± 0.021 m w.e. yr^{-1} from 2000 to 2012. In order to compare our estimate with that for the east Kunlun Mts. and inner Tibet in Gardner et al. (2013), we excluded the result of the western Kunlun Mts. and retrieved the mean glacier mass change in the other 21 study sites in the INTP. Our estimated glacier mass balance of -0.041 ± 0.014 m w.e. yr^{-1} between 2000 and 2012 is supported by that of 2003–2009 (-0.01 ± 0.11 m w.e. yr^{-1}) [14]. However, Brun et al. (2017) detected a negative glacier mass change of -0.15 ± 0.24 m w.e. yr^{-1} between 2000 and 2016 for the inner TP [18]. The difference between our estimate and the result in Brun et al. (2017) may be partly attributed to a possible bias due to the limited available optical images caused by snow or cloud cover.

Overall, our retrieved negative mass change in the mountain glaciers in the INTP is basically less than that in the Himalaya Mts. [18], Qilian Mts. [7] and southeastern TP [45]. It indicates that glaciers in the INTP were relatively more stable than those in the surrounding mountains. However, glacier mass losses of some glacierized areas in the INTP such as Geladandong Mts. [42], Puruogangri ice field [39] and Xiaodongkemadi Glacier [46] were accelerated in recent years. These published results cannot prove the generalization of accelerated mass loss to other INTP glaciers because of the heterogeneous glacier responses to climate change [7]. Consequently, it is necessary to estimate the recent glacier mass

balances of other glacierized regions to investigate the temporal changes in regional mass balances over the INTP.

5.2. Glacier Anomalous Regions in the HMA

Glacier anomaly, which is opposed to the worldwide pronounced glacier mass loss in recent decades, is featured by glacier mass gain or balanced glacier mass change [8–10]. Therefore, the estimated decade-average glacier mass gain indicates the existence of glacier anomaly during the studied period, at least for some years. For the INTP, we detected that the spatial variation in glacier mass balances between 2000 and 2012 is apparently characterized by negative mass changes in the southeast and positive mass changes in the northwest (Figure 8). Similar spatial variations in glacier mass changes have also been detected over the neighboring mountains of the Pamir, Karakoram, Himalaya Mts. and southeastern TP [7,10,45]. Our detected glacier mass gains apparently indicate the existence of glacier anomalous phenomenon in the northwestern part or even central part of the INTP. This means that the glacier anomaly phenomenon may have existed in the interior region of the TP since the early 21st century. Moreover, we infer that the southeastern boundary of glacier anomalous regions may be located over the central zone of the INTP (Zone B in Figure 8).

In order to further analyze the coverage of anomalous regions for the HMA between 2000 and 2012, we employed the previously published geodetic glacier mass balance estimates of the neighboring mountains of the INTP during the similar time period. By comparing the SPOT DEMs and SRTM DEM, glacier mass changes between 1999 and 2011 were detected for nine study sites in the neighboring mountains [9]. In this study, we only used the estimates of the four study sites in the Himalaya Mts. For more detailed results, we also employed the geodetic glacier mass balances from 2000 to 2014 over ten study sites of the Pamir and Karakoram Mts. [10]. Moreover, we employed the geodetic estimates between 2000 and the 2010s of six glacierized regions in the southeastern TP [45]. By visually interpreting our estimations of the INTP and the published geodetic results in the neighboring mountains (Figure 11), we inferred that the center of glacier anomalous regions is possibly located over the western Kunlun Mts. Consequently, it is likely that the PKWK glacier anomaly will be renamed the Western Kunlun Centered (WKC) glacier anomaly, at least in the period from 2000 to 2012.

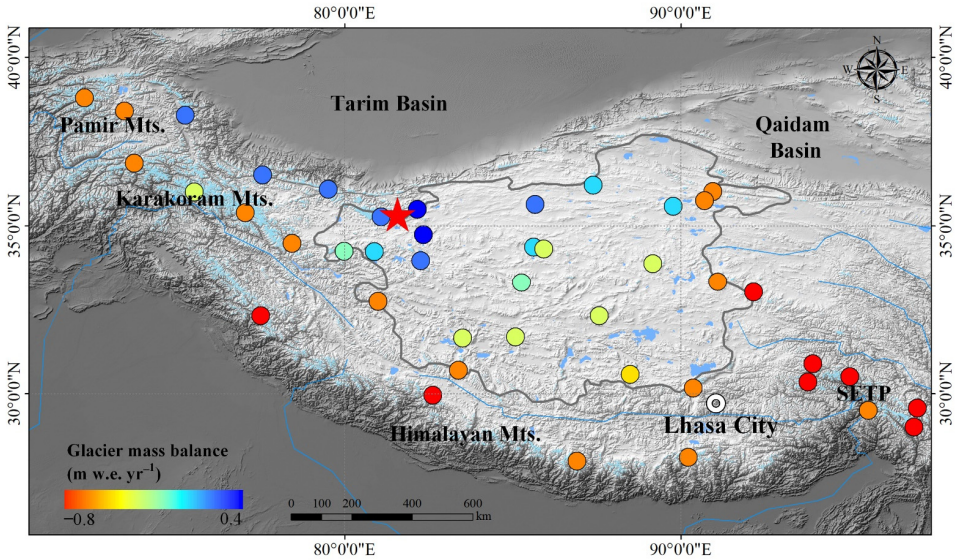

Figure 11. Our measured results of the INTP and the previously published geodetic estimates in the Pamir, Karakoram, Himalaya Mts. and southeastern TP (SETP). The red star, which is located at the western Kunlun Mts., represents the possible center of glacier anomalous regions which is estimated with a visual interpretation.

5.3. Impact of Atmospheric Circulations in the TP

The large-scale anomalous regions imply that the observed glacier anomaly may be attributed to a regional climatic anomaly [11]. Basically, the climate conditions of TP and its surroundings are mainly determined by two atmospheric circulations of the Indian summer monsoon and the mid-latitude westerlies [17]. It has been found that the glacier anomaly in the Karakoram, Pamir and western Kunlun Mts. is mainly attributed to the strengthened westerlies which leads to an increasing winter precipitation [10,17]. Therefore, the coverage of glacier anomaly is possibly related to the domain of westerlies. This suggests that the blue dashed line in Figure 8 could be the southeastern limit of mid-latitude westerlies in recent decades. Furthermore, the red dashed line in Figure 8 could be the northwestern boundary of the Indian monsoon, according to the fact that the weakening monsoon probably causes regional glacier mass loss [45].

The boundaries of mid-latitude westerlies and Indian summer monsoon have also been detected by analyzing the transport of atmospheric water vapor [47,48] and records of stable oxygen isotopes in precipitation [25,49]. Recently, according to the stable oxygen isotopes data of 18 meteorological stations, the TP was classified into three distinct parts of westerlies domain (north of 35°N), transition area (from 30°N to 35°N) and monsoon domain (south of 30°N) [24]. Note that only four meteorological stations are located over the INTP, and thus the whole INTP was classified into a transition zone. In this study, our results did not contradict that estimated from stable oxygen isotope data. However, with the observations of glacier mass balances in 22 study sites of the INTP, we were able to delineate more precise boundaries for westerlies and monsoon domains. This result is significant for interpreting climatic conditions and hydrological processes in the plateau and for projecting the glacier's response to regional climate changes.

Although a southeastern limit for mid-latitude westerlies or a northwestern limit for the Indian summer monsoon was detected, we still agree to that mid-latitude westerlies are a possible climatic control in monsoon-dominated regions and vice versa. The high mountain valleys in the TP and its surroundings may provide some pathways for the Indian summer monsoon and mid-latitude westerlies [50]. For example, glacier mass change in the Zhadang Glacier (30°N) over the southern part of the INTP could be affected by the intensity of mid-latitude westerlies dynamics [51]. Furthermore, the Indian monsoon could be another control of regional climatic conditions in the northern TP [52]. Additionally, during the winter season, mid-latitude westerlies are major climatic factor of the whole TP, as Indian monsoon only occurs in summer [53].

6. Conclusions

This study presents geodetic glacier mass balance estimates of the INTP between 2000 and 2012, in order to investigate the southeastern limit of the PKWK glacier anomaly. The DEM differencing processing and related error corrections were conducted on the SRTM DEM and the generated TanDEM-X DEMs. Based on mountain glacier distributions, 22 glacierized regions were selected in the INTP. We estimated decade-average glacier mass balances ranging from -0.339 ± 0.040 to 0.237 ± 0.078 m w.e. yr^{-1} over these 22 glacierized regions. Among them, nine study sites (e.g., the Songzhi peak and western Kunlun) experienced glacier mass gain, whereas we measured glacier mass losses for the other thirteen glacierized regions such as the Nainqentanglha and Geladandong Mts. Overall, the average glacier mass balance of 0.018 ± 0.021 m w.e. yr^{-1} was determined across the INTP.

The spatial variation in glacier mass balance is characterized by glacier mass gain for the northwestern part and glacier mass loss for the southeastern part. This suggests that glacier anomaly may have existed over the northwestern or even central region of the INTP since the early 21st century. The southeastern boundary of glacier anomaly may have been located over the inner area of the INTP during the studied period. Our glacier mass balance estimates and the published geodetic results in the neighboring mountains indicate that the center of glacier anomalous regions may be located over the western Kunlun Mts. In recent years, accelerated glacier mass loss has been detected for some glacierized regions

in the southeastern area of the INTP. Therefore, the measurements of recent mass changes in the northwestern and central zones of the INTP are needed to investigate the temporal changes in glacier anomalous regions.

Author Contributions: Conceptualization, L.J. and H.W.; methodology, L.L. and Y.S.; validation, L.L. and L.J.; formal analysis, L.L. and H.W.; data curation, L.L. and Y.S.; writing—original draft preparation, L.L.; writing—review and editing, L.J. and H.W.; visualization, L.L.; funding acquisition, L.J. and H.W. All authors have read and agreed to the published version of the manuscript.

Funding: This research was funded by the National Key Research and Development Program, grant number 2017YFA0603103, the National Natural Science Foundation of China, grant number 41704023, 42174046 and 41974009, the Key Research Program of Frontier Sciences, Chinese Academy of Sciences, grant number QYZDB-SSW-DQC027 and QYZDJ-SSW-DQC042, and the Strategic Priority Research Program of the Chinese Academy of Sciences, grant number XDA19070104.

Data Availability Statement: The current article.

Acknowledgments: The authors thank the German Aerospace Center (DLR) for providing the TanDEM-X InSAR data sets and the SRTM-X DEM, the United States Geological Survey (USGS) for providing the SRTM-C DEM and the National Aeronautics and Space Administration (NASA) for providing the Landsat optical images.

Conflicts of Interest: The authors declare no conflict of interest.

References

1. Wouters, B.; Gardner, A.S.; Moholdt, G. Global glacier mass loss during the grace satellite mission (2002–2016). *Front. Earth Sci.* **2019**, *7*, 96. [CrossRef]
2. Zemp, M.; Huss, M.; Thibert, E.; Eckert, N.; McNabb, R.; Huber, J.; Barandun, M.; Machguth, H.; Nussbaumer, S.U.; Gärtner-Roer, I.; et al. Global glacier mass changes and their contributions to sea-level rise from 1961 to 2016. *Nature* **2019**, *568*, 382–386. [CrossRef] [PubMed]
3. Song, C.; Huang, B.; Richards, K.; Ke, L.; Hien Phan, V. Accelerated lake expansion on the Tibetan Plateau in the 2000s: Induced by glacial melting or other processes? *Water Resour. Res.* **2014**, *50*, 3170–3186. [CrossRef]
4. Yao, T.; Li, Z.; Yang, W.; Guo, X.; Zhu, L.; Kang, S.; Wu, Y.; Yu, W. Glacial distribution and mass balance in the Yarlung Zangbo River and its influence on lakes. *Chin. Sci. Bull.* **2010**, *55*, 2072–2078. [CrossRef]
5. Pritchard, H.D. Asia's glaciers are a regionally important buffer against drought. *Nature* **2017**, *545*, 169–174. [CrossRef]
6. Pritchard, H.D. Asia's shrinking glaciers protect large populations from drought stress. *Nature* **2019**, *569*, 649–654. [CrossRef]
7. Shean, D.E.; Bhushan, S.; Montesano, P.M.; Rounce, D.R.; Arendt, A.; Osmanoglu, B. A systematic, regional assessment of high mountain Asia glacier mass balance. *Front. Earth Sci.* **2020**, *7*, 363. [CrossRef]
8. Gardelle, J.; Berthier, E.; Arnaud, Y. Slight mass gain of Karakoram glaciers in the early twenty-first century. *Nat. Geosci.* **2012**, *5*, 322–325. [CrossRef]
9. Gardelle, J.; Berthier, E.; Arnaud, Y.; Kääb, A. Region-wide glacier mass balances over the Pamir-Karakoram-Himalaya during 1999–2011. *Cryosphere* **2013**, *7*, 1263–1286. [CrossRef]
10. Lin, H.; Li, G.; Cuo, L.; Hooper, A.; Ye, Q. A decreasing glacier mass balance gradient from the edge of the Upper Tarim Basin to the Karakoram during 2000–2014. *Sci. Rep.* **2017**, *7*, 6712. [CrossRef]
11. Kääb, A.; Treichler, D.; Nuth, C.; Berthier, E. Brief communication: Contending estimates of 2003–2008 glacier mass balance over the Pamir-Karakoram-Himalaya. *Cryosphere* **2015**, *9*, 557–564. [CrossRef]
12. Zhou, Y.; Li, Z.; Li, J.; Zhao, R.; Ding, X. Glacier mass balance in the Qinghai-Tibet Plateau and its surroundings from the mid-1970s to 2000 based on Hexagon KH-9 and SRTM DEMs. *Remote Sens. Environ.* **2018**, *210*, 96–112. [CrossRef]
13. Guo, W.; Liu, S.; Xu, J.; Wu, L.; Shangguan, D.; Yao, X.; Wei, J.; Bao, W.; Yu, P.; Liu, Q.; et al. The second Chinese glacier inventory: Data, methods and results. *J. Glaciol.* **2015**, *61*, 357–372. [CrossRef]
14. Gardner, A.S.; Moholdt, G.; Cogley, J.G.; Wouters, B.; Arendt, A.A.; Wahr, J.; Berthier, E.; Hock, R.; Pfeffer, W.T.; Kaser, G.; et al. A reconciled estimate of glacier contributions to sea level rise: 2003 to 2009. *Science* **2013**, *340*, 852–857. [CrossRef] [PubMed]
15. Treichler, D.S.; Kääb, A. Icesat laser altimetry over small mountain glaciers. *Cryosphere* **2016**, *10*, 2129–2146. [CrossRef]
16. Neckel, N.; Kropáček, J.; Bolch, T.; Hochschild, V. Glacier mass changes on the Tibetan Plateau 2003–2009 derived from ICESat laser altimetry measurements. *Environ. Res. Lett.* **2014**, *9*, 014009. [CrossRef]
17. Yao, T.; Thompson, L.; Yang, W.; Yu, W.; Gao, Y.; Guo, X.; Yang, X.; Duan, K.; Zhao, H.; Xu, B.; et al. Different glacier status with atmospheric circulations in Tibetan Plateau and surroundings. *Nat. Clim. Chang.* **2012**, *2*, 663–667. [CrossRef]
18. Brun, F.; Berthier, E.; Wagnon, P.; Kääb, A.; Treichler, D. A spatially resolved estimate of High Mountain Asia glacier mass balances from 2000 to 2016. *Nat. Geosci.* **2017**, *10*, 668–673. [CrossRef]

19. Berthier, E.; Arnaud, Y.; Kumar, R.; Ahmad, S.; Wagnon, P.; Chevallier, P. Remote sensing estimates of glacier mass balances in the Himachal Pradesh (western Himalaya, India). *Remote Sens. Environ.* **2007**, *108*, 327–338. [CrossRef]
20. Wu, K.; Liu, S.; Jiang, Z.; Xu, J.; Wei, J.; Guo, W. Recent glacier mass balance and area changes in the Kangri Karpo Mountains from DEMs and glacier inventories. *Cryosphere* **2018**, *12*, 103–121. [CrossRef]
21. Neckel, N.; Braun, A.; Kropáček, J.; Hochschild, V. Recent mass balance of the Purogangri Ice Cap, central Tibetan Plateau, by means of differential X-band SAR interferometry. *Cryosphere* **2013**, *7*, 1623–1633. [CrossRef]
22. Liu, G.; Fan, J.; Zhao, F.; Mao, K.; Dou, C. Monitoring elevation change of glaciers on Geladandong Mountain using TanDEM-X SAR interferometry. *J. Mt. Sci.* **2017**, *14*, 859–869. [CrossRef]
23. Li, G.; Lin, H. Recent decadal glacier mass balances over the western Nyainqentanglha Mountains and the increase in their melting contribution to Nam Co Lake measured by differential bistatic SAR interferometry. *Glob. Planet. Chang.* **2017**, *149*, 177–190. [CrossRef]
24. Yao, T.; Masson-Delmotte, V.; Gao, J.; Yu, W.; Yang, X.; Risi, C.; Sturm, C.; Werner, M.; Zhao, H.; He, Y.; et al. A review of climatic controls on δ18o in precipitation over the Tibetan Plateau: Observations and simulations. *Rev. Geophys.* **2013**, *51*, 525–548. [CrossRef]
25. Tian, L.; Yao, T.; MacClune, K.; White, J.W.C.; Schilla, A.; Vaughn, B.; Vachon, R.; Ichiyanagi, K. Stable isotopic variations in west China: A consideration of moisture sources. *J. Geophys. Res.* **2007**, *112*, D10112. [CrossRef]
26. Maussion, F.; Scherer, D.; Mölg, T.; Collier, E.; Curio, J.; Finkelnburg, R. Precipitation seasonality and variability over the Tibetan Plateau as resolved by the high Asia reanalysis. *J. Clim.* **2014**, *27*, 1910–1927. [CrossRef]
27. Jiang, L.; Nielsen, K.; Andersen, O.B.; Bauer-Gottwein, P. Monitoring recent lake level variations on the Tibetan Plateau using CryoSat-2 SARIn mode data. *J. Hydrol.* **2017**, *544*, 109–124. [CrossRef]
28. Zhang, G.; Yao, T.; Xie, H.; Zhang, K.; Zhu, F. Lakes' state and abundance across the Tibetan Plateau. *Chin. Sci. Bull.* **2014**, *59*, 3010–3021. [CrossRef]
29. Zhang, G.; Xie, H.; Kang, S.; Yi, D.; Ackley, S.F. Monitoring lake level changes on the Tibetan Plateau using ICESat altimetry data (2003–2009). *Remote Sens. Environ.* **2011**, *115*, 1733–1742. [CrossRef]
30. Lei, Y.; Yao, T.; Bird, B.W.; Yang, K.; Zhai, J.; Sheng, Y. Coherent lake growth on the central Tibetan Plateau since the 1970s: Characterization and attribution. *J. Hydrol.* **2013**, *483*, 61–67. [CrossRef]
31. Wei, J.; Liu, S.; Guo, W.; Yao, X.; Xu, J.; Bao, W.; Jiang, Z. Surface-area changes of glaciers in the Tibetan Plateau interior area since the 1970s using recent Landsat images and historical maps. *Ann. Glaciol.* **2014**, *55*, 213–222.
32. Zhou, Y.; Hu, J.; Li, Z.; Li, J.; Zhao, R.; Ding, X. Quantifying glacier mass change and its contribution to lake growths in central Kunlun during 2000–2015 from multi-source remote sensing data. *J. Hydrol.* **2019**, *570*, 38–50. [CrossRef]
33. Liu, L.; Jiang, L.; Sun, Y.; Yi, C.; Wang, J.; Hsu, H. Glacier elevation changes (2012–2016) of the Puruogangri Ice Field on the Tibetan Plateau derived from bi-temporal TanDEM-X InSAR data. *Int. J. Remote Sens.* **2016**, *37*, 5687–5707. [CrossRef]
34. Rabus, B.; Eineder, M.; Roth, A.; Bamler, R. The shuttle radar topography mission—a new class of digital elevation models acquired by spaceborne radar. *ISPRS J. Photogramm. Remote Sens.* **2003**, *57*, 241–262. [CrossRef]
35. Nuth, C.; Kääb, A. Co-registration and bias corrections of satellite elevation data sets for quantifying glacier thickness change. *Cryosphere* **2011**, *5*, 271–290. [CrossRef]
36. Berthier, E.; Arnaud, Y.; Baratoux, D.; Vincent, C.; Rémy, F. Recent rapid thinning of the "Mer de Glace" glacier derived from satellite optical images. *Geophys. Res. Lett.* **2004**, *31*, L17401. [CrossRef]
37. Huss, M. Density assumptions for converting geodetic glacier volume change to mass change. *Cryosphere* **2013**, *7*, 877–887. [CrossRef]
38. Kääb, A.; Berthier, E.; Nuth, C.; Gardelle, J.; Arnaud, Y. Contrasting patterns of early twenty-first-century glacier mass change in the Himalayas. *Nature* **2012**, *488*, 495–498. [CrossRef]
39. Liu, L.; Jiang, L.; Jiang, H.; Wang, H.; Ma, N.; Xu, H. Accelerated glacier mass loss (2011–2016) over the Puruogangri Ice Field in the inner Tibetan Plateau revealed by bistatic InSAR measurements. *Remote Sens. Environ.* **2019**, *231*, 111241. [CrossRef]
40. Lambrecht, A.; Mayer, C.; Wendt, A.; Floricioiu, D.; Völksen, C. Elevation change of Fedchenko Glacier, Pamir Mountains, from GNSS field measurements and TanDEM-X elevation models, with a focus on the upper glacier. *J. Glaciol.* **2018**, *64*, 637–648. [CrossRef]
41. Li, S.; Yao, T.; Yang, W.; Yu, W.; Zhu, M. Glacier energy and mass balance in the inland Tibetan Plateau: Seasonal and interannual variability in relation to atmospheric changes. *J. Geophys. Res.* **2018**, *123*, 6390–6409. [CrossRef]
42. Liu, L.; Jiang, L.; Zhang, Z.; Wang, H.; Ding, X. Recent accelerating glacier mass loss of the Geladandong Mountain, inner Tibetan Plateau, estimated from ZiYuan-3 and TanDEM-X measurements. *Remote Sens.* **2020**, *12*, 472. [CrossRef]
43. Guo, W.; Liu, S.; Wei, J.; Bao, W. The 2008/09 surge of central Yulinchuan Glacier, northern Tibetan Plateau, as monitored by remote sensing. *Ann. Glaciol.* **2013**, *54*, 299–310. [CrossRef]
44. Huintjes, E.; Neckel, N.; Hochschild, V.; Schneider, C. Surface energy and mass balance at Purogangri Ice Cap, central Tibetan Plateau, 2001–2011. *J. Glaciol.* **2015**, *61*, 1048–1060. [CrossRef]
45. Ke, L.; Song, C.; Yong, B.; Lei, Y.; Ding, X. Which heterogeneous glacier melting patterns can be robustly observed from space? A multi-scale assessment in southeastern Tibetan Plateau. *Remote Sens. Environ.* **2020**, *242*, 111777. [CrossRef]
46. Zhang, Z.; Jiang, L.; Liu, L.; Sun, Y.; Wang, H. Annual glacier-wide mass balance (2000–2016) of the interior Tibetan Plateau reconstructed from MODIS albedo products. *Remote Sens.* **2018**, *10*, 1031. [CrossRef]

47. Shi, Y. Characteristics of late Quaternary monsoonal glaciation on the Tibetan Plateau and in East Asia. *Quat. Int.* **2002**, *97*, 79–91. [CrossRef]
48. Chen, F.; Chen, J.; Holmes, J.; Boomer, I.; Austin, P.; Gates, J.B.; Wang, N.; Brooks, S.J.; Zhang, J. Moisture changes over the last millennium in arid central Asia: A review, synthesis and comparison with monsoon region. *Quat. Sci. Rev.* **2010**, *29*, 1055–1068. [CrossRef]
49. Johnson, K.R.; Ingram, B.L. Spatial and temporal variability in the stable isotope systematics of modern precipitation in China: Implications for paleoclimate reconstructions. *Earth Planet. Sci. Lett.* **2004**, *220*, 365–377. [CrossRef]
50. Bookhagen, B.; Burbank, D.W. Toward a complete Himalayan hydrological budget: Spatiotemporal distribution of snowmelt and rainfall and their impact on river discharge. *J. Geophys. Res.* **2010**, *115*, F03019. [CrossRef]
51. Mölg, T.; Maussion, F.; Scherer, D. Mid-latitude westerlies as a driver of glacier variability in monsoonal high Asia. *Nat. Clim. Chang.* **2014**, *4*, 68–73. [CrossRef]
52. Yang, M.; Yao, T.; Wang, H.; Tian, L.; Gou, X. Estimating the criterion for determining water vapour sources of summer precipitation on the northern Tibetan Plateau. *Hydrol. Process.* **2006**, *20*, 505–513. [CrossRef]
53. Curio, J.; Maussion, F.; Scherer, D. A 12-year high-resolution climatology of atmospheric water transport over the Tibetan Plateau. *Earth Syst. Dyn.* **2015**, *6*, 109–124. [CrossRef]